EUROPEAN COMMISSION

Community research

Fast / Instant Release of Safety Relevant Radionuclides from Spent Nuclear Fuel FIRST-Nuclides

COLLABORATIVE PROJECT (CP)
(Contract Number: FP7-295722)

Characterisation of spent UO_2 fuel used for experimental work in FIRST-Nuclides

Deliverable No: 1.3

Author(s): D. H. Wegen, D. Papaioannou, R. Nasyrow, R. Gretter, G. Paperini, S. van Winckel, D. Serrano Purroy, A. Martínez Torrens, R. Sureda, A. Schubert, V. V. Rondinella, J. P. Glatz and V. Metz

Reporting period: 1/Jul./2013 – 15/Dec./2014

Date of issue of this report : 18. Dec./2014

Start date of project : **1/Jan./2012** Duration : 36 Months

DISTRIBUTION LIST

[FIRST-Nuclides]

FIRST Nuclides

EURATOM

Name	Number of copies	Comments

Project co-funded by the European Commission under the Seventh Euratom Framework Programme for Nuclear Research &Training Activities (2007-2011)		
Dissemination Level		
PU	Public	X
RE	Restricted to a group specified by the partners of [FIRST-Nuclides]	
CO	Confidential, only for partners of the [FIRST-Nuclides] project	

Table of contents

List of tables

List of figures

1. Introduction

The EURATOM FP7 Collaborative Project "Fast/Instant Release of Safety Relevant Radionuclides from Spent Nuclear Fuel (FIRST-Nuclides)" aims to provide new and comprehensive knowledge of the fast / instantly released radionuclides from disposed high burn-up spent UO_2 fuel. The fast release of a specific fraction radionuclides will take place only after a canister failure and water penetration to the spent nuclear fuel (SNF) in a repository. The so-called instant release fraction (IRF) consists of radionuclides in gaseous form, and radionuclides showing a high solubility in groundwater.

The basic activities of the project FIRST-Nuclides – coordinated in workpackage #1 "Samples and Tools" - were to select, provide and prepare SNF samples for subsequent experimental investigations. The objectives of this workpackage included the complete characterization of the selected SNF materials with respect to the individual fuel characteristics and irradiation history, achieving permission by the fuel owners for publication of key parameters as well as the installation of experimental and analytical tools. All experimentally working partners of the FIRST-Nuclides project (i.e. KIT, JRC-ITU, JÜLICH, PSI, SCK•CEN, CNRS, CTM, MTA EK and STUDSVIK) contributed to this workpackage. Initially the activities within workpackage #1 were planned to be conducted until June 2013 and the respective achievements are documented in deliverables D1.1 *Characterisation of spent nuclear fuel samples to be used in FIRST-Nuclides – relevance of samples for the Safety Case* [1] and D1.2 *Characterisation of spent nuclear fuel samples and description of methodologies and tools to be applied in FIRST-Nuclides* [2] of FIRST-Nuclides.

Since there were delays in the documentation and with the sample preparation of SNF materials used by JRC-ITU and CTM, these institutions continued their activities within workpackage #1. This deliverable D1.3 presents an up-dated characterisation of the two commercial BWR fuels (denoted as BWR42 and BWR54) with average burn-up of 42 GWd/t_{HM} and 54 GWd/t_{HM}, respectively. These SNF have been selected for leaching experiments by JRC-ITU and CTM in WP3 and oxygen diffusion experiments in WP2 by JRC-ITU. The main emphasis is on chemical analyses of the radionuclide inventories of the SNF samples, which are compared to the respective inventories calculated by means of the KORIGEN code. In addition ceramography results obtained from the PWR fuel rod segments SBS1108 N0204 (50.4 GWd/t_{HM}) are reported. This SNF has been used for leaching experiments in WP3 and gas-release analyses in WP2 by KIT.

2. Calculated centreline temperatures of spent nuclear fuels BWR42 and BWR54

In addition to the irradiation data of the BWR fuels BWR42 and BWR54 reported in [3] the centreline temperature at the position of the fuel samples (as maximum and average for each irradiation cycle) is given in *Figure 1*. The data of BWR42 have been reported by the utility while the temperature profile of BWR54 was estimated from irradiation power history data using the TRANSURANUS code. The maximum temperature for both fuels was around 1100°C. In the first 1500 hours irradiation time the average was between ~700°C to ~1000°C.

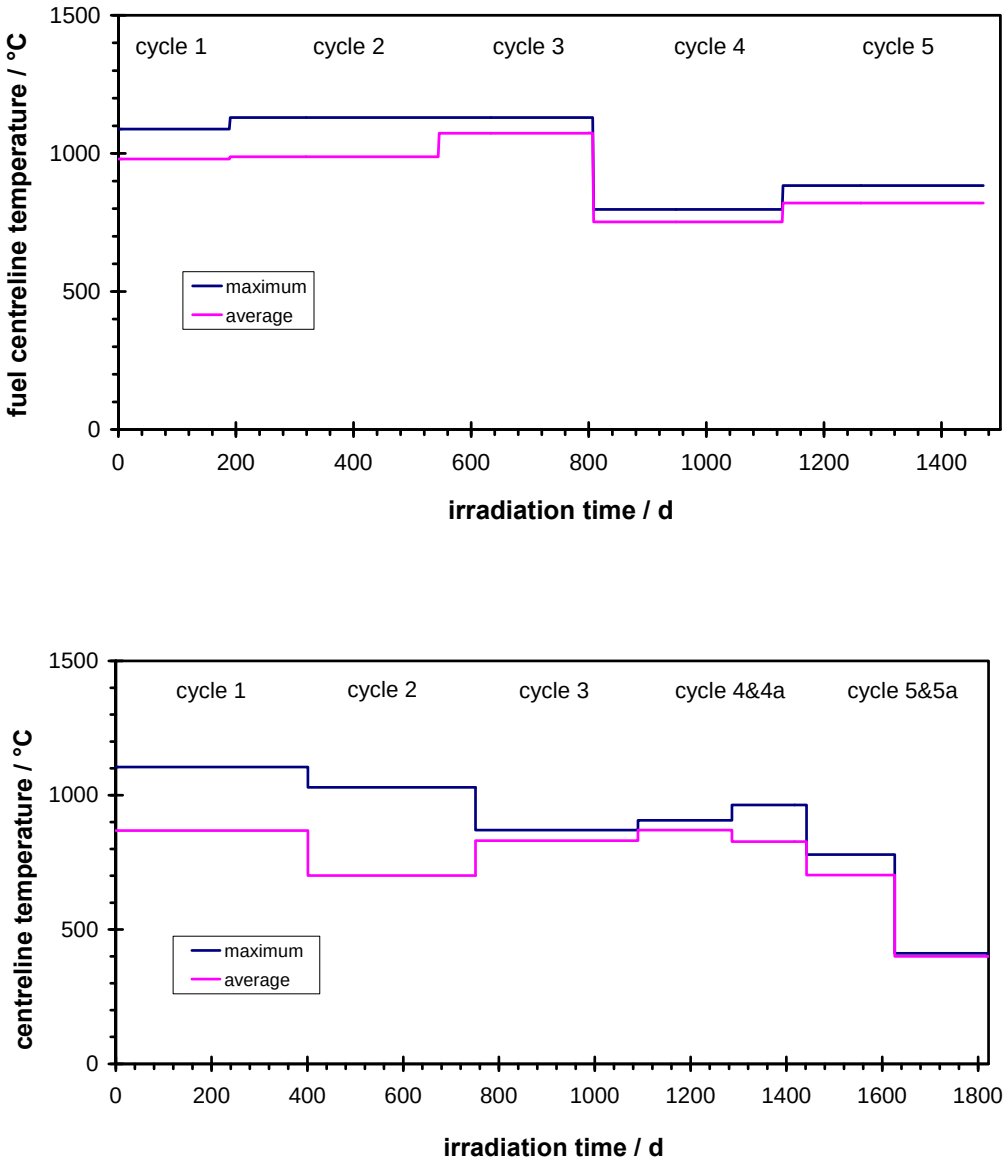

Figure 1: Fuel centreline temperature – maximum and average values of each irradiation cycle – at sample position of BWR42 fuel (upper diagram) and BWR54 fuel (lower diagram).

3. Experimental inventory determination of spent nuclear fuels BWR42 and BWR54

3.1. Experimental

The inventory of radionuclides was determined experimentally for the BWR42 and BWR54 fuels. For each fuel the inventory determination was performed for a cladded segment, powder from the centre (IN) and from the periphery of the pellet (OUT). The experimental determination was performed using ICP-MS and γ-spectrometry.

To determine experimentally the powder inventories, approximately 0.05 g of powder were dissolved in acid using a Parr Teflon bomb. Each powder was dissolved in two different acidic media: in 30 mL of 0.1 M HF in concentrated HNO_3 solution at 210°C and in 30 mL of a mixture HNO_3:HCl (180:70 volume ratio) at 180°C. Both dissolution experiments lasted 12 hours. After the experiments no solid parts were observed. Cladded segment inventory determination experiments were made using a flask of 250 ml using 8 M nitric acid. The experiments were carried during 5 hours at 110-135°C. After the heating the solution was filtered in order to remove the cladding. Dilutions 1/10000 and 1/100000 were analysed using ICP-MS. Also the last dilution was analysed by γ-spectrometry.

3.2. Results

The experimental inventory results are given in *Table 1* and *Table 2*. Calculated (KORIGEN) inventories are also given for comparison.

Table 1: Radionuclide inventory for BWR42 fuel.

Element	IN	OUT	Pellet	Theoretical
	$\frac{\mu g}{g_{fuel}}$	$\frac{\mu g}{g_{fuel}}$	$\frac{\mu g}{g_{fuel}}$	$\frac{\mu g}{g_{fuel}}$
Rb	400 ± 30	400 ± 20	200 ± 30	400
Sr	1100 ± 40	1200 ± 50	1600 ± 150	800
Y	500 ± 35	700 ± 45	500 ± 100	500
Zr	4500 ± 150	5700 ± 150	4700 ± 300	4200
Mo	3800 ± 150	4800 ± 200	3600 ± 500	3800
Tc	800 ± 50	1100 ± 50	800 ± 100	900
Ru	2400 ± 100	3000 ± 150	1700 ± 300	2300
Rh	500 ± 25	700 ± 45	300 ± 60	500
Pd	1400 ± 150	2600 ± 200	2300 ± 500	1600
Cs	2800 ± 100	3300 ± 150	2600 ± 300	2700
Ba	7700 ± 250	4300 ± 150	2100 ± 1800	2100
La	1500 ± 50	1900 ± 100	1500 ± 200	1400
Ce	2700 ± 100	3400 ± 150	2700 ± 300	2700
Pr	1300 ± 50	1800 ± 100	1300 ± 200	1300
Nd	5500 ± 300	6900 ± 400	5500 ± 1000	4400
Sm	1000 ± 150	1200 ± 100	1200 ± 400	1000
U	844500 ± 12500	826500 ± 9000	823800 ± 24000	833500
Np	600 ± 50	900 ± 50	600 ± 100	500
Pu	10500 ± 350	13000 ± 500	10800 ± 1000	8700
Am	200 ± 20	500 ± 45	300 ± 90	800
Cm	40 ± 10	100 ± 25	100 ± 40	30

According to *Table 1*, in the case of the BWR42 spent nuclear fuel, the experimental inventory of the cladded segment is not significantly different to the calculated values. However, both powder fractions present significant differences. In the periphery of the fuel (OUT sample) the uranium content is lower, whereas the minor actinides (MAn) and the fission products (FP) are more abundant than the calculated values. On the contrary, in the centre of the fuel (IN sample) the results are the opposite, more uranium and less MAn and FP content than the calculated values are found. These results are not surprising and can be explained based on the local differences in burn-up and neutron capture, as well as, for some elements like Cs, on the segregation and redistribution during the irradiation according to the temperature profile in the pellets.

In the case observed in *Table 2*, the uranium inventory of the BWR54 cladded segment is slightly higher than the calculated and the powder values. In addition, the uranium determined in both powder fractions is also higher than the calculated value. However, the FPs behave similarly to the previous sample. An effort will be dedicated to understand this unforeseen behaviour and improve the reliability of the uranium results. Indeed, the ICPMS measurements present a higher uncertainty for these samples than usual and short after the measurement the instrument broke down. Samples will be measured again once the instrument is repaired.

Despite the differences between the calculated and the experimental data, the ratio between the different elements for the powder fractions and the pellets is correct and similar to the elemental ratio in the calculated inventory.

Table 2: Radionuclide inventory for BWR54 fuel.

Element	IN	OUT	Pellet	Theoretical
	$\frac{\mu g}{g_{fuel}}$	$\frac{\mu g}{g_{fuel}}$	$\frac{\mu g}{g_{fuel}}$	$\frac{\mu g}{g_{fuel}}$
Rb	400 ± 80	500 ± 90	700 ± 120	500
Sr	1300 ± 680	1500 ± 780	1300 ± 700	1100
Y	600 ± 120	800 ± 150	700 ± 140	600
Zr	5100 ± 1000	7400 ± 1500	6100 ± 1200	5200
Mo	4300 ± 1200	7600 ± 2100	4700 ± 1300	4800
Tc	1000 ± 200	1400 ± 300	1000 ± 200	1100
Ru	2800 ± 600	4200 ± 900	2600 ± 500	3100
Rh	500 ± 130	900 ± 210	600 ± 150	600
Pd	1700 ± 700	1400 ± 500	3500 ± 1300	2200
Cs	3300 ± 600	4600 ± 800	3900 ± 600	3700
Ba	5700 ± 1500	5000 ± 1300	3700 ± 1000	2600
La	1700 ± 300	2600 ± 500	2200 ± 400	1800
Ce	3000 ± 600	4600 ± 900	3600 ± 700	3500
Pr	1500 ± 300	2300 ± 500	2000 ± 400	1600
Nd	6200 ± 1100	9200 ± 1700	7300 ± 1300	5600
Sm	1500 ± 300	2500 ± 600	2100 ± 500	1200
U	856300 ± 44000	873600 ± 45000	909800 ± 47000	822400
Np	1100 ± 100	1300 ± 200	1300 ± 200	600
Pu	9800 ± 1800	13900 ± 2500	11500 ± 2100	8900
Am	100 ± 50	300 ± 110	200 ± 70	600
Cm	100 ± 40	200 ± 90	100 ± 60	100

4. Burn-up calculations based on overview analysis results

4.1. Methodology

The local burn-up of a spent nuclear fuel sample (expressed in %FIMA, Fissions per Initial Metal Atom) is most frequently derived from the radiochemical analysis result of the burn-up indicator ^{148}Nd, accurately measured by isotope dilution mass spectrometry [4]. As the determination of ^{148}Nd by mass spectrometry is hampered by the isobaric interference from ^{148}Sm, a preliminary Nd/Sm separation is needed.

At ITU, ^{148}Nd used to be accurately measured by Inductively Coupled Plasma – Mass Spectrometry (ICP-MS) using isotope dilution, preceded by on-line Ion Chromatography (IC) for the Nd/Sm separation. Unfortunately, the old instrument used for this set-up had broken down and needed replacement. A new instrument has been bought but the installation got delayed so that the determination of ^{148}Nd as burn-up indicator via IC-ICP-MS using isotope dilution became impossible within the timeframe for the First Nuclides project.

As an alternative approach, the burn-up of the two spent fuel samples has been calculated with the overview analysis results of the dissolved spent fuel samples (without any separation) and using ^{139}La, $^{143+144}$Nd and $^{145+146}$Nd respectively as burn-up indicators. In the mass spectrometric analysis, these nuclides (except ^{144}Nd) do not suffer from isobaric interferences. The isobaric interference from ^{144}Ce on ^{144}Nd in these older spent fuel samples does not play a role as in fact the sum of both nuclides (= *mass* 144 concentration) is the value that counts. The non-negligible conversion of ^{143}Nd to ^{144}Nd and ^{145}Nd to ^{146}Nd in a thermal neutron flux precludes the independent use of these burn-up indicators. As overview analysis results using external calibration are *de facto* less accurate and precise than dedicated analysis results using isotope dilution, the resulting uncertainty on the calculated burn-up with these data will not be better than ±10%.

For each burn-up indicator, the average weighted fission yield must be calculated. In order to do so, the 'fissile' composition of the fuel (= ^{235}U, ^{239}Pu and ^{241}Pu; assuming all fissions come from these three nuclides) should be known at any moment during irradiation. As this is practically impossible, two different approaches have been used to calculate the average weighted fission yields [5].

A. The average 'fissile' composition of the fuel is calculated as the arithmetic mean of the composition at the start of irradiation (given by the manufacturer of the fuel) and the composition at the end of irradiation (result of the radiochemical overview analysis).

B. The average 'fissile' composition or the fission contribution of each of the fissile nuclides is determined from the ratio of two fission isotopes with sufficiently different fission yields for the different fissile nuclides. The ^{148}Nd/^{150}Nd ratio is such an example. It reflects the continuous change in 'fissile' composition.

As input data the results from the overview analyses have been used, not only for the mentioned burn-up indicators but also for the ^{148}Nd/^{150}Nd ratio and for the actinides. More specifically, the ^{148}Nd/^{150}Nd ratio and the concentrations of the fissile nuclides ^{235}U, ^{239}Pu and ^{241}Pu are needed for the calculation of the average weighted fission yields of the burn-up indicators and the sum of all actinides is needed for the %FIMA calculation. ORIGEN calculations (using the nominal burn-up of the fuel pin) were used to resolve the isobaric

interferences at mass 241 (Pu/Am), and for approach B, also for masses 148 and 150 (both Nd/Sm interferences). Only the calculated mass ratios of the interfering nuclides were used to resolve these interferences, and the resulting isotopic compositions of the elements (Pu, Am, Nd and Sm) were checked versus the expected theoretical ones. Although these checks confirmed the expected isotopic compositions, it remains a tricky point in these calculations that theoretical results (for a given burn-up) are needed to confirm later on the experimental burn-up.

4.2. Results of burn-up calculations

The results for both fuel samples are given in *Table 3* with average weighted fission yields calculated according to approach A and in *Table 4* with average weighted fission yields calculated according to approach B. Both approaches confirm each other nicely (well within the abovementioned uncertainty). Whereas approach A is the more simple one, approach B needs (in this case) more calculated theoretical input (ORIGEN calculations). A better agreement between the different burn-up indicators could be hoped for, independent from the chosen approach A or B. But the differences according to burn-up monitor rather reflect the higher uncertainty levels of the used analytical results. All burn-up results confirm the expected burn-up of the spent fuel samples.

Table 3: Burn-up results for both fuel samples using approach A for the calculation of the average weighted fission yields: via linear interpolation between 'fissile' fuel composition at the start and at the end of irradiation.

Fuel sample	Burn-up indicator	No. of atoms atoms/g_{fuel}	Fission Yield atoms/100f	Burn-up at% FIMA
BWR42	Mass 143+144	$1.05 \cdot 10^{19}$	10.37	4.5
	$^{145+146}$Nd	$6.95 \cdot 10^{18}$	6.482	4.7
	^{139}La	$6.24 \cdot 10^{18}$	6.216	4.5
			Avg BU	**4.6**
BWR54	Mass 143+144	$1.26 \cdot 10^{19}$	10.38	5.4
	$^{145+146}$Nd	$8.20 \cdot 10^{18}$	6.486	5.6
	^{139}La	$7.47 \cdot 10^{18}$	6.217	5.3
			Avg BU	**5.4**

Table 4: Burn-up results for both fuel samples using approach B for the calculation of the average weighted fission yields: with fission contributions of ^{235}U, ^{239}Pu and ^{241}Pu calculated via the $^{148}Nd/^{150}Nd$ ratio.

Fuel sample	Burn-up indicator	No. of atoms atoms/g_{fuel}	Fission Yield atoms/100f	Burn-up at% FIMA
BWR42	Mass 143+144	$1.05 \cdot 10^{19}$	10.62	4.4
	$^{145+146}$Nd	$6.95 \cdot 10^{18}$	6.584	4.7
	^{139}La	$6.24 \cdot 10^{18}$	6.248	4.4
			Avg BU	**4.5**
BWR54	Mass 143+144	$1.26 \cdot 10^{19}$	10.18	5.5
	$^{145+146}$Nd	$8.20 \cdot 10^{18}$	6.393	5.7
	^{139}La	$7.47 \cdot 10^{18}$	6.194	5.4
			Avg BU	**5.5**

As mentioned in the inventory results, the overview measurements were less precise than usual but shortly after the measurements, the instrument broke down. The samples will be measured again once the instrument is repaired. Moreover, once a new instrument will be successfully installed, dedicated burn-up measurements of these samples (including separations) are envisaged.

5. SEM characterisation of BWR42 and BWR54 powder samples

Samples were obtained from powders of the BWR42 and BWR54 fuels. For each fuel was powder from the centre (CORE) and the periphery (OUT) of the pellet prepared. The powder was milled and sieved. A fraction of powder with diameters larger than 50 μm was characterised by SEM and is used for the corrosion experiments. The SEM characterisation will be repeated when the corrosion experiments are finalised.

The SEM micrographs are shown in *Figure 2* and *Figure 3*.

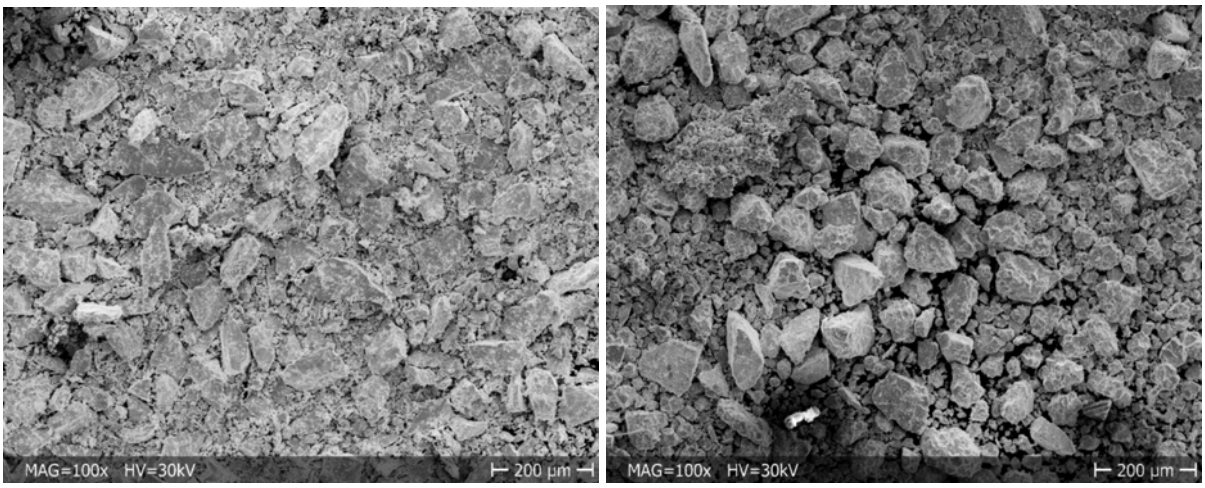

Figure 2: BWR42 powder from the CORE fraction (left) and from the OUT fraction (right).

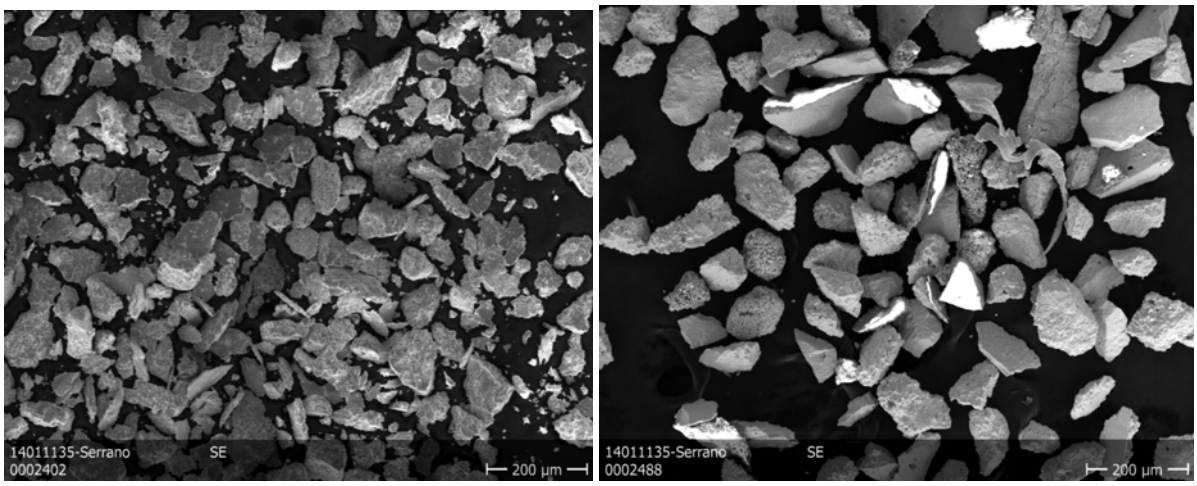

Figure 3: BWR54 powder from the CORE fraction (left) and from the OUT fraction (right).

A large difference in the number of fines located on the small fuel fragments can be observed between BWR42 and BWR54 fuel. The BWR54 fuel powders were prepared using a sieving machine while the BWR42 fuel powders had to be sieved manually because the sieving machine broke down.

From the SEM measurements the particle size was calculated (Table 5). For each particle the length in the X axis and the Y axis was measured and the total average was calculated.

Particles smaller than 20 µm were not taken into account since they are considered to be removed in the first experimental washing.

Table 5: Particle size of the different fuel fractions.

Sample	Particle size µm
BWR42 - CORE	50±20
BWR42 - OUT	46±20
BWR54 - CORE	73±28
BWR54 - OUT	91±37

Details of the particles are shown in *Figure 4* and *Figure 5*. It is clearly seen that the porosity in the OUT fraction particles is higher than in the CORE fraction of the fuels.

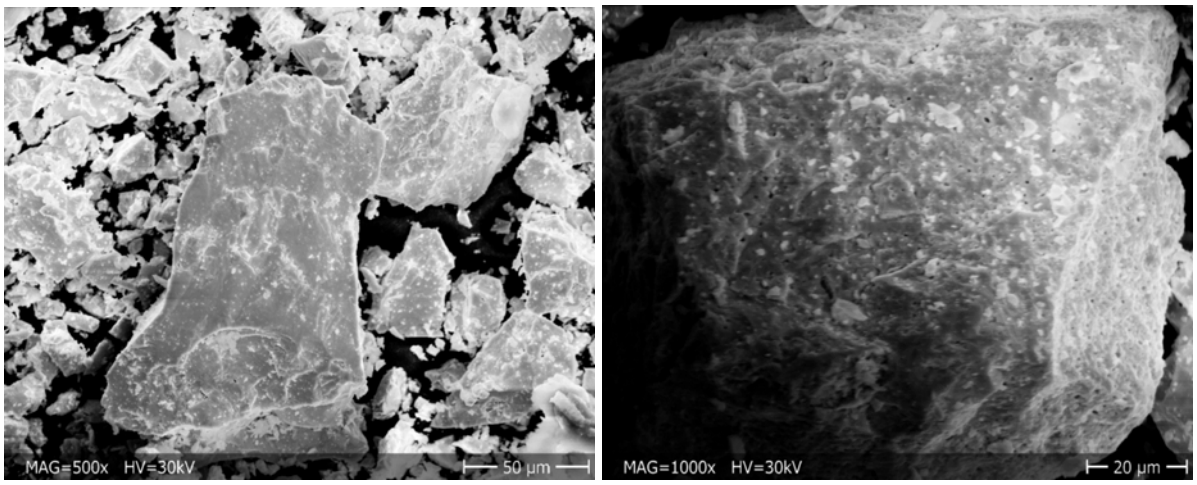

Figure 4: BWR42 particles from the CORE fraction (left) and from the OUT fraction (right).

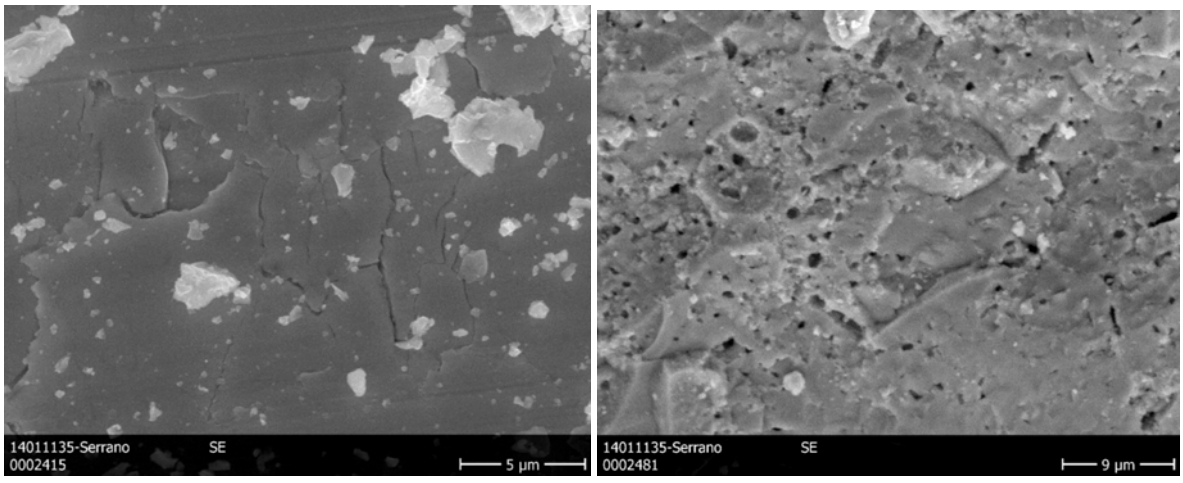

Figure 5: BWR54 particles from the CORE fraction (left) and from the OUT fraction (right).

6. Ceramography of samples of the PWR fuel rod segment SBS1108-N0204

6.1. Samples

In the 1980s, a series of fuel rod segments were irradiated in the Swiss Gösgen PWR (KKG) to analyze the performance of UO_2 fuels, which had been fabricated with different sintering and gelation manufacturing methods. For each irradiation test, five segments and additional dummy segments were mounted to make a full-length KKG fuel rod. The fuel of rod SBS1108 was fabricated by Kraftwerk Union AG. Most fuel pellets had been initially enriched with 3.8 wt.% ^{235}U in segment N0204 of the fuel rod. In each of the fuel rod segments with NIKUSI pellets, two pellets adjacent to the upper and lower isolation pellets were made of U_{nat} (*Figure 6*). The fuel rod SBS1108 was irradiated in four cycles for 1226 days total irradiation, which started in 1985 and ended on May 27, 1989. Segment N0204 achieved an average burn-up of 50.4 GWd/t_{HM}; an average linear heat generation rate of 260 $W \cdot cm^{-1}$ is reported for SBS1108 N0204.

The procedures used for characterisation and cutting of the fuel samples are described in [6] and [7]. The positions of the samples used for ceramography are given in *Figure 6*. The irradiated enriched UO_2 samples are designated as #1021and #1022, while #1023 is irradiated natural UO_2. The local burn-up at the positions of the samples was estimated from the ratio of the locally measured ^{137}Cs activity [6], [9] (see *Table 6*).

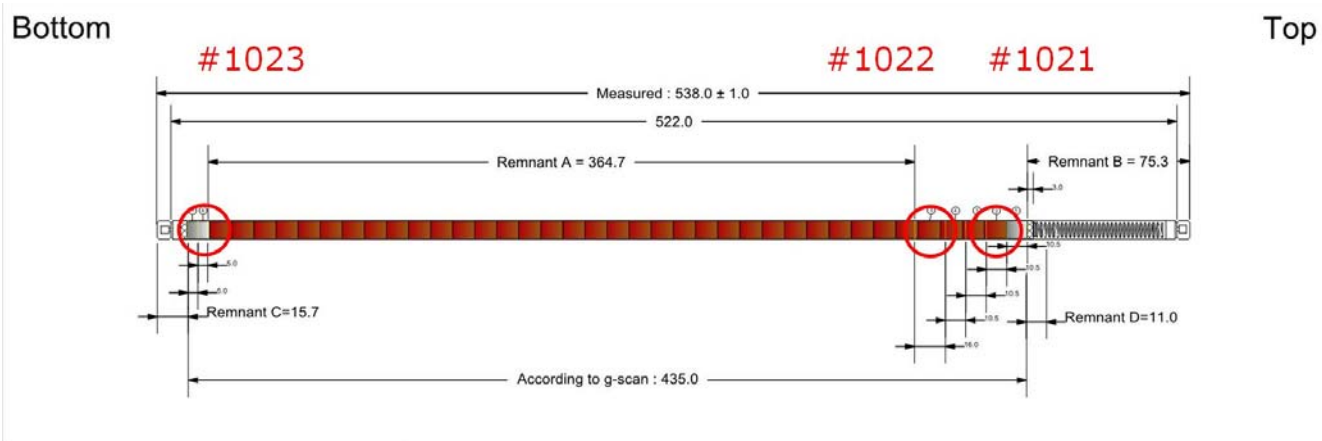

Figure 6: Cutting plan of segment N0204 of SBS 1108 showing the positions of microscopy samples #1021, #1022 (enriched UO_2 pellets) and #1023 (natural UO_2). Surfaces pointing to the top side of the segment were subject to ceramography.

Table 6: Estimated burn-up of samples #1021, #1022 and #1023.

	#1023	#1021 & #1022	ratio(#1021/#1023)
Material	nat. UO_2	UO_2 fuel	
Enrichment(%)	0.7	3.8	5.4
Activity of Cs-137 (a.u.)	2.3 10^9	3.1 10^9	1.4
estim. BU(GWd/t)	~36	~50	

Sample #1021 and #1023 are radial cut while #1022 is cut axial. Coordinates to describe locations on the samples are given as relative coordinates to the radius r_0 (x_0 in case of #1022) and the angle (sample length y_0 in case of #1022) as shown in *Figure 7* and *Figure 8*.

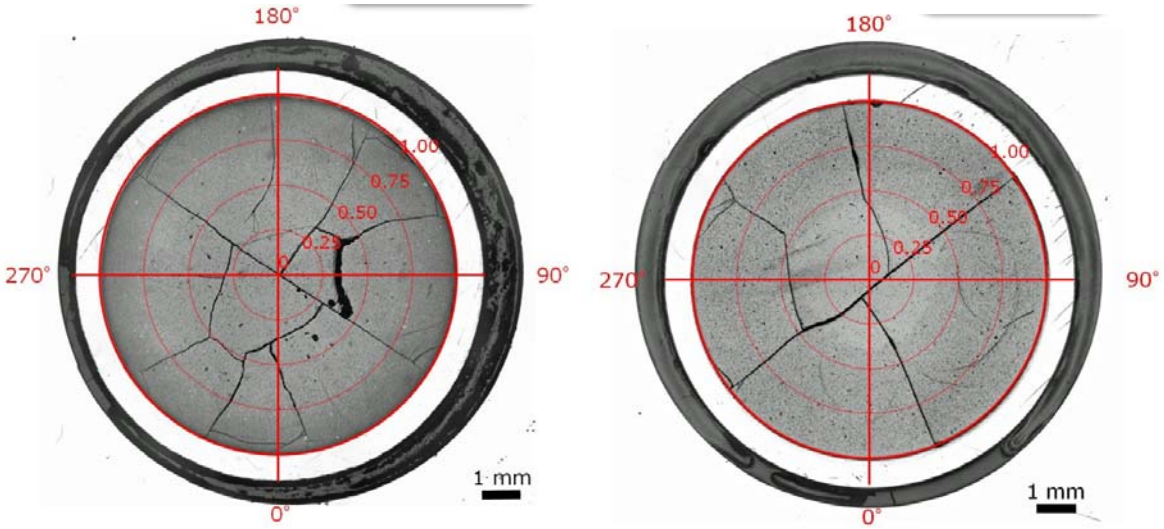

Figure 7: Macrographs of radial cut samples #1021(left) and #1023(right) including coordinates (red) used as reference for ceramography.

The fuel samples cut for optical microscopy were embedded in epoxy resin (Struers, Denmark) in cylindrical aluminium holders in which grooves had been machined in the upper and lower parts to facilitate handling by manipulators. Each sample was fixed in place in the aluminium holder using double-sided adhesive tape and the epoxy resin was fed drop-wise into the holder through a small plastic tube. A plastic collar was fixed around the top of the holder to avoid excess resin running down the sides. To ensure that the resin completely impregnated the sample, embedding was carried out under vacuum (0.2 bar). This was carried out in a small polyethylene chamber which was evacuated using a miniature pump (Vacuum-Set-Universal, Type 9117) marketed by SCAN-DIA, Hagen, Germany.

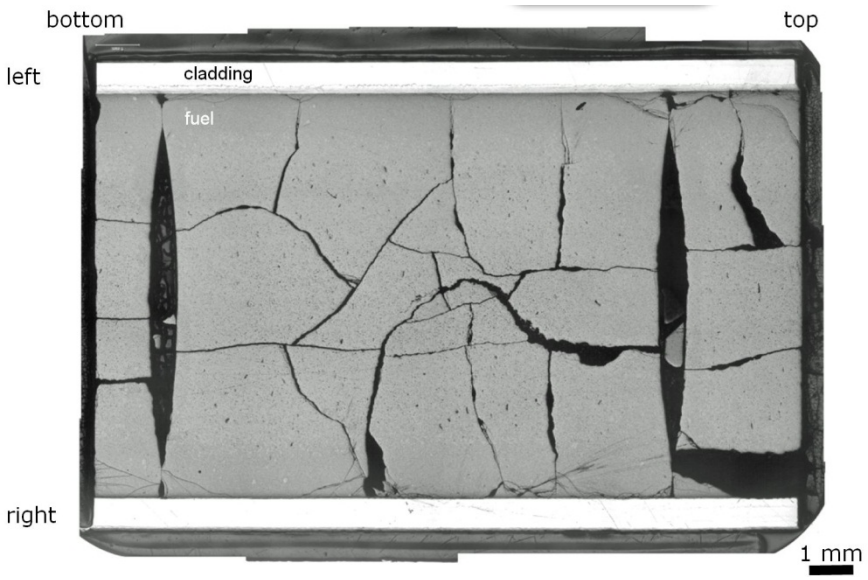

Figure 8: Macrograph of axial cut sample #1022. The horizontal axis is referred as y-axis (0 at bottom end of the sample) while the vertical axis is referred as x-axis (0 in the centre).

Standard metallographic practice was employed. Fine grinding of the sample was carried out using 75 micron diamond paper (Kulzer, Germany) and water as a lubricant. Grinding was followed by polishing with a series of water-based diamond powder suspensions of increasing fineness (particle size: 15, 6, 3 and 1 micron). For grinding and polishing, the sample was contained in a compartment of a special cassette and held against the rotating disc of the grinding/polishing machine by the addition of weights. Prior to examination in the optical microscope and between each preparation step, the sample was washed in Mecaprex GH, a commercial, ethanol containing, wash medium marketed by Presi, France.

The fuel samples were examined using a Leica Telatom-3 light optical microscope. The microscope is connected to the sample preparation cell by a conveyor belt. The first step in the examination of each sample was the preparation of an optical macrograph. This was obtained by assembling six to twelve individual digital images of magnification 20x using a computer program from Leica. For all samples, the fuel microstructure was recorded at the pellet surface (r/r_0=1; x/x_0=1), r/r_0=0.75, r/r_0=0.50, r/r_0= 0.25, and at the pellet centre (r/r_0= 0). This was done for #1021 and #1023 at two angles (0° and 90°) and for #1022 at two heights (y/y_0=0.53 and y/y_0=0.79)(see *Figure 7*and *Figure 8*).

6.2. Outer oxide layer

The thickness of the external oxide layer on the cladding was determined from at least 12 micrographs taken at locations along the claddings outer surface. On each micrograph the oxide thickness was measured at multiple points. On micrographs with the outer oxide edge out of focus an uncertainty was estimated taking into account the transition width from grey to black. In some cases the outer edge could not be seen, here the visible thickness is given marked as *oxide thickness larger than data value*. Thickness measurements were made using the UTHSCSA *ImageTool* program [10]. Examples are shown in

Figure 9 and *Figure 11*.

The results for the thickness of the external oxide layer are given in *Figure 10*, *Figure 12* and *Figure 13*. It can be seen that the average thickness of the oxide for the samples from the top end of the fuel stack is consistent ~48 µm (#1021, #1022). Some micrographs were poor and lead to deviating results which were not taken into account for the average oxide thickness

data. The natural UO_2 sample #1023 from the bottom end of the fuel stack shows a lower oxide thickness of 26 µm reflecting the lower burn-up and temperature at this location. The optical microscopy results show a trend similar to the results obtained by Eddy Current (ECT) measurements [8]. It has however to be noted that the thickness measured on the micrographs tend to be larger for #1021 and #1022 than that obtained by ECT measurements at the same positions (35 and 39 µm).

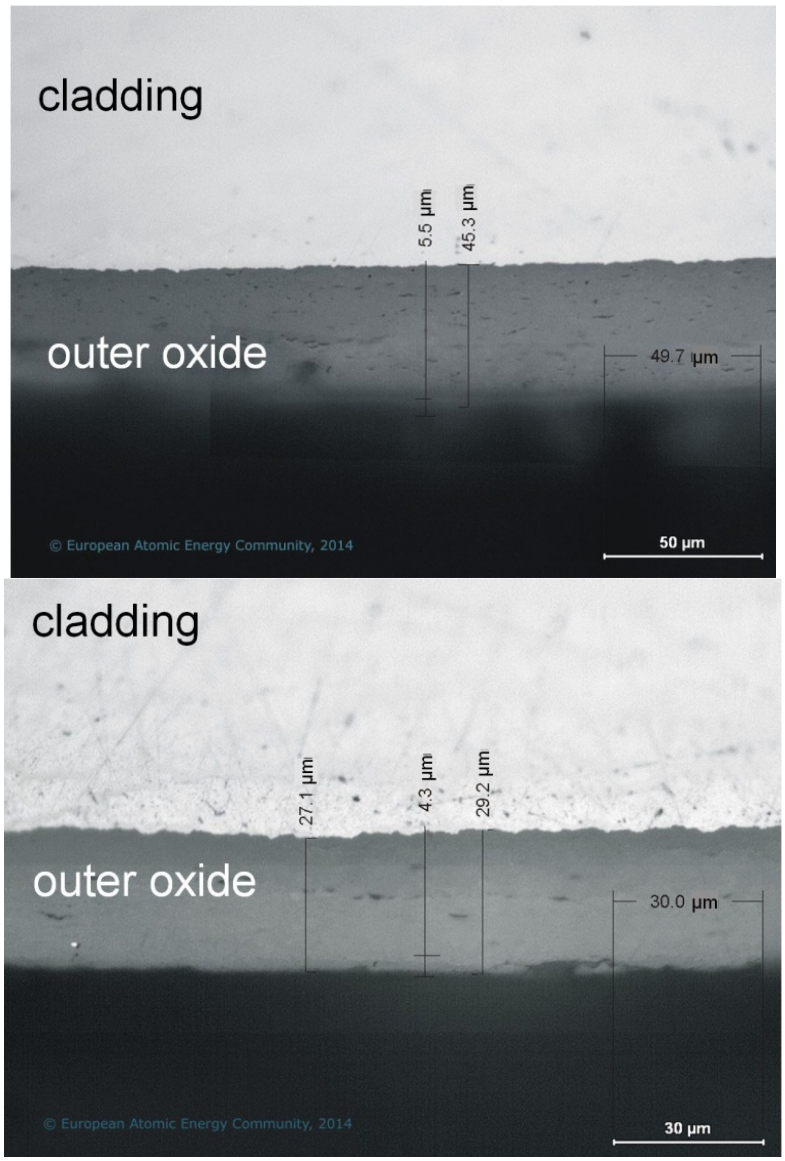

Figure 9: Micrograph of the outer oxide layer of the cladding of sample #1021 at 303° (upper image) and of sample #1023 at 260° (lower image).

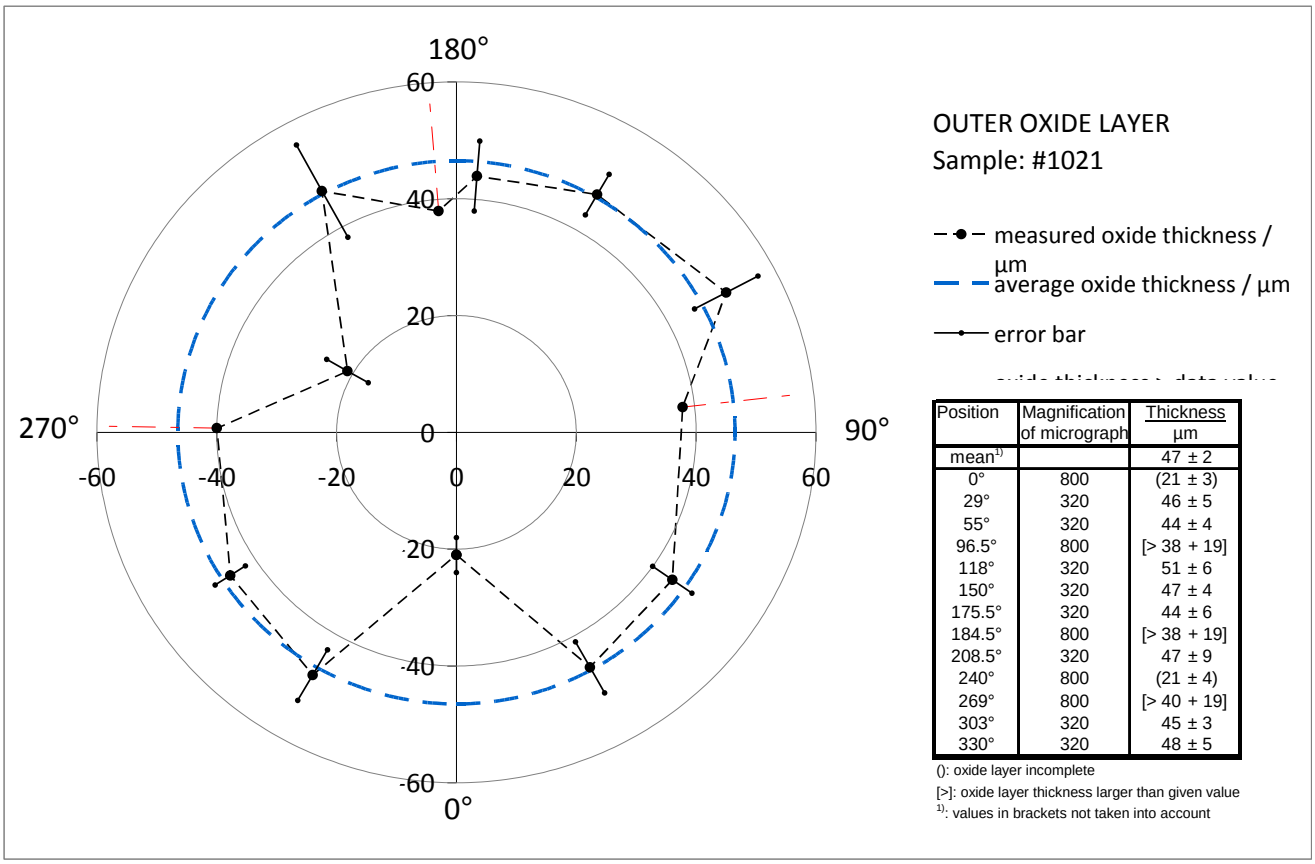

Position	Magnification of micrograph	Thickness µm
mean[1)]		47 ± 2
0°	800	(21 ± 3)
29°	320	46 ± 5
55°	320	44 ± 4
96.5°	800	[> 38 + 19]
118°	320	51 ± 6
150°	320	47 ± 4
175.5°	320	44 ± 6
184.5°	800	[> 38 + 19]
208.5°	320	47 ± 9
240°	800	(21 ± 4)
269°	800	[> 40 + 19]
303°	320	45 ± 3
330°	320	48 ± 5

(): oxide layer incomplete
[>]: oxide layer thickness larger than given value
[1)]: values in brackets not taken into account

Figure 10: Thickness of the outer oxide layer on the cladding of sample #1021.

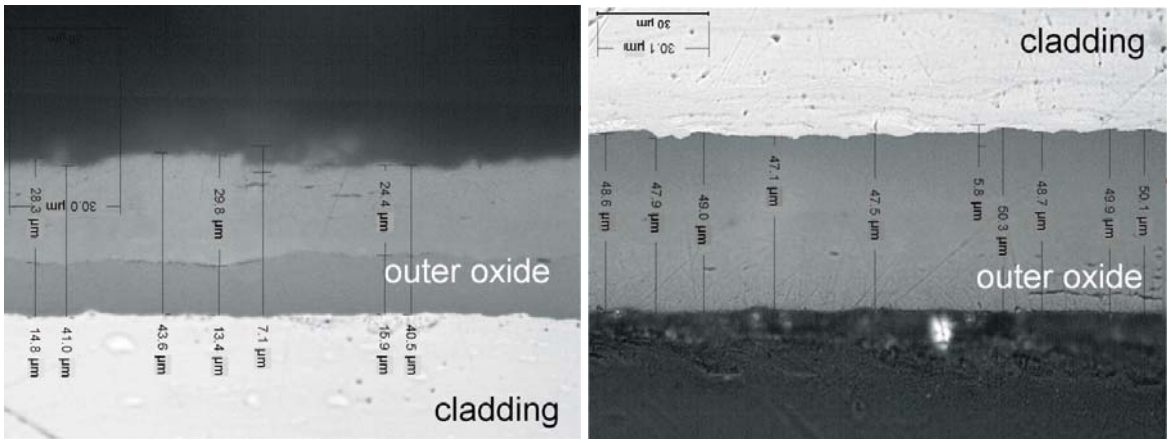

Figure 11: Micrograph of the outer oxide layer of the cladding of sample #1022 at left position y=3.4 mm (left image) and at right position y=15.6 mm (right image).

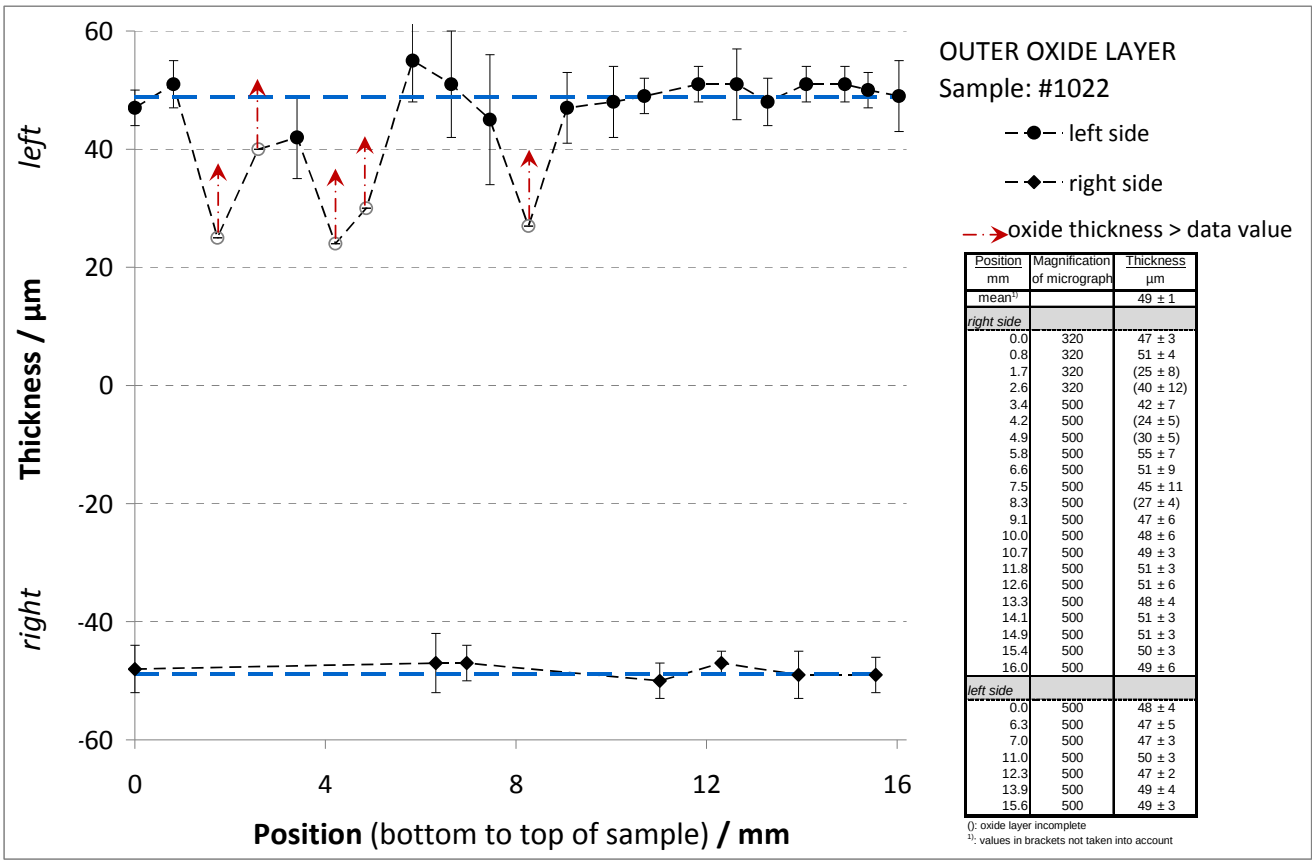

Position mm	Magnification of micrograph	Thickness µm
mean[1)]		49 ± 1
right side		
0.0	320	47 ± 3
0.8	320	51 ± 4
1.7	320	(25 ± 8)
2.6	320	(40 ± 12)
3.4	500	42 ± 7
4.2	500	(24 ± 5)
4.9	500	(30 ± 5)
5.8	500	55 ± 7
6.6	500	51 ± 9
7.5	500	45 ± 11
8.3	500	(27 ± 4)
9.1	500	47 ± 6
10.0	500	48 ± 6
10.7	500	49 ± 3
11.8	500	51 ± 3
12.6	500	51 ± 6
13.3	500	48 ± 4
14.1	500	51 ± 3
14.9	500	51 ± 3
15.4	500	50 ± 3
16.0	500	49 ± 6
left side		
0.0	500	48 ± 4
6.3	500	47 ± 5
7.0	500	47 ± 3
11.0	500	50 ± 3
12.3	500	47 ± 2
13.9	500	49 ± 4
15.6	500	49 ± 3

(): oxide layer incomplete
1): values in brackets not taken into account

Figure 12: Thickness of the outer oxide layer on the cladding of sample #1022.

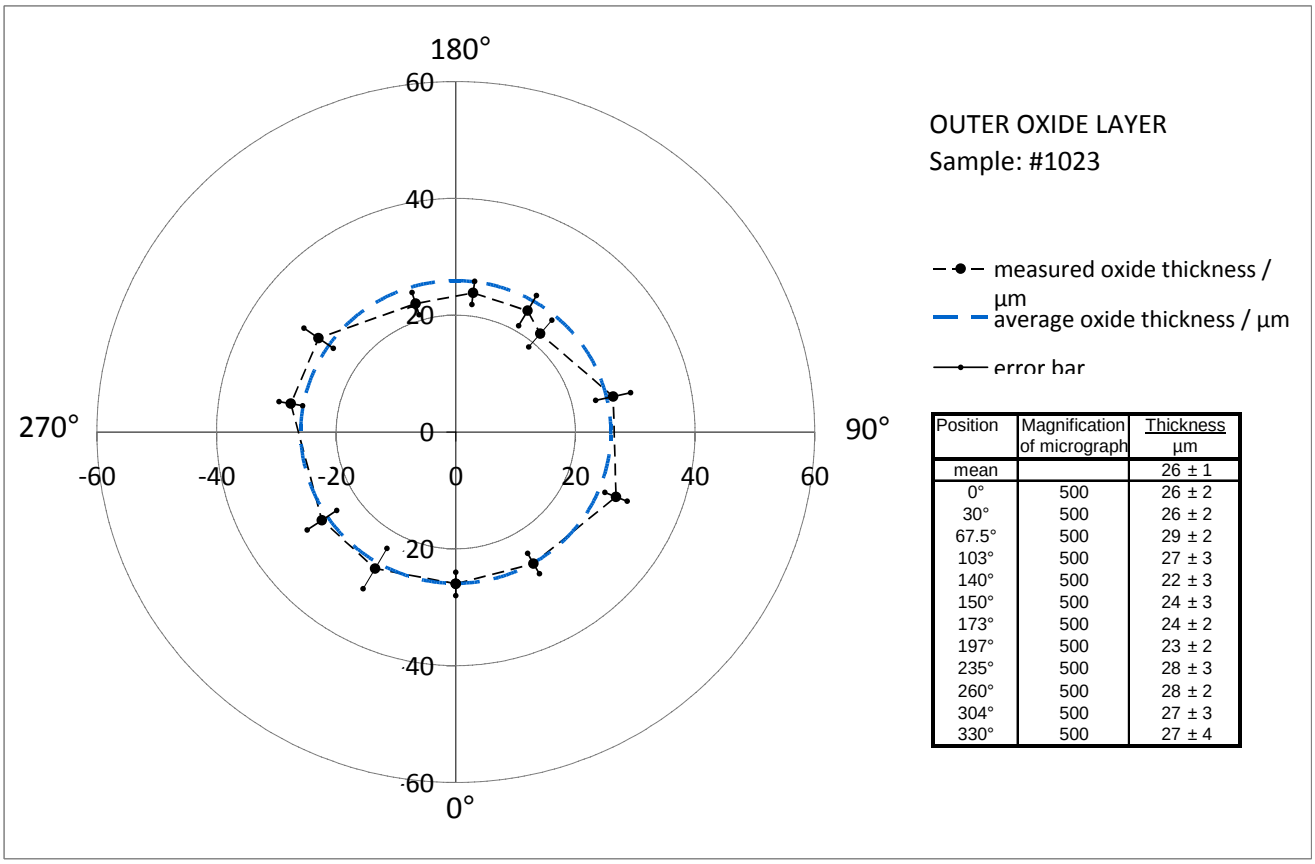

Position	Magnification of micrograph	Thickness µm
mean		26 ± 1
0°	500	26 ± 2
30°	500	26 ± 2
67.5°	500	29 ± 2
103°	500	27 ± 3
140°	500	22 ± 3
150°	500	24 ± 3
173°	500	24 ± 2
197°	500	23 ± 2
235°	500	28 ± 3
260°	500	28 ± 2
304°	500	27 ± 3
330°	500	27 ± 4

Figure 13: Thickness of the outer oxide layer on the cladding of sample #1023

6.3. Pellet cladding interaction zone

Figure 14 and

Figure 15 show the pellet cladding interaction zone with the internal oxide layer. The gap between fuel and cladding is closed at the top end of the fuel stack (#1021, #1022). Here is the internal oxide layer detached from the cladding and the fuel is cracked along the cladding. At the bottom end (#1023) were the burn-up is lower the gap is not closed and where inner oxide is present it is attached to the cladding.

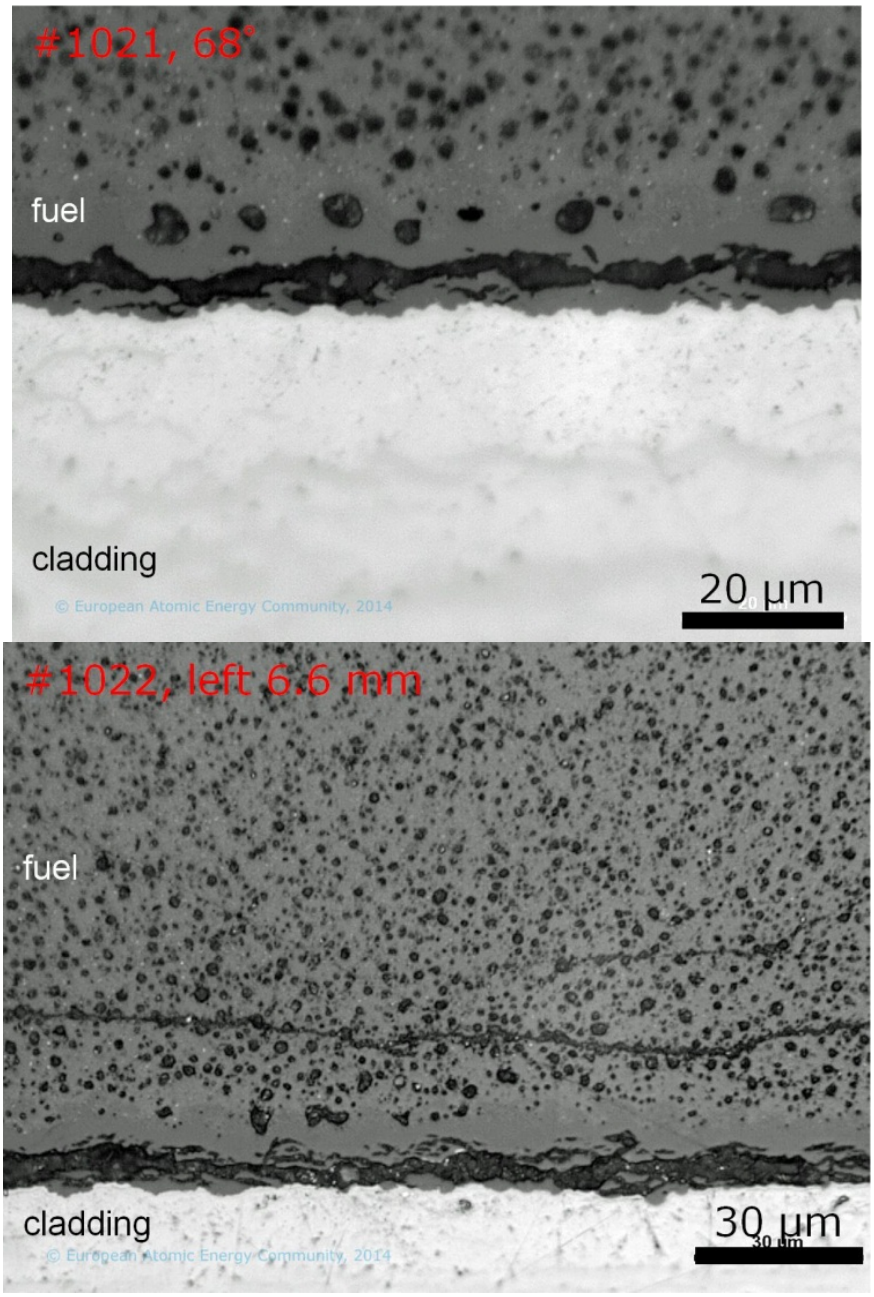

Figure 14: Micrographs of the PCI zones of the radial cut sample #1021 (upper image) and the axial cut sample #1022 (lower image) at 68° and positon left y=6.6 mm, respectively.

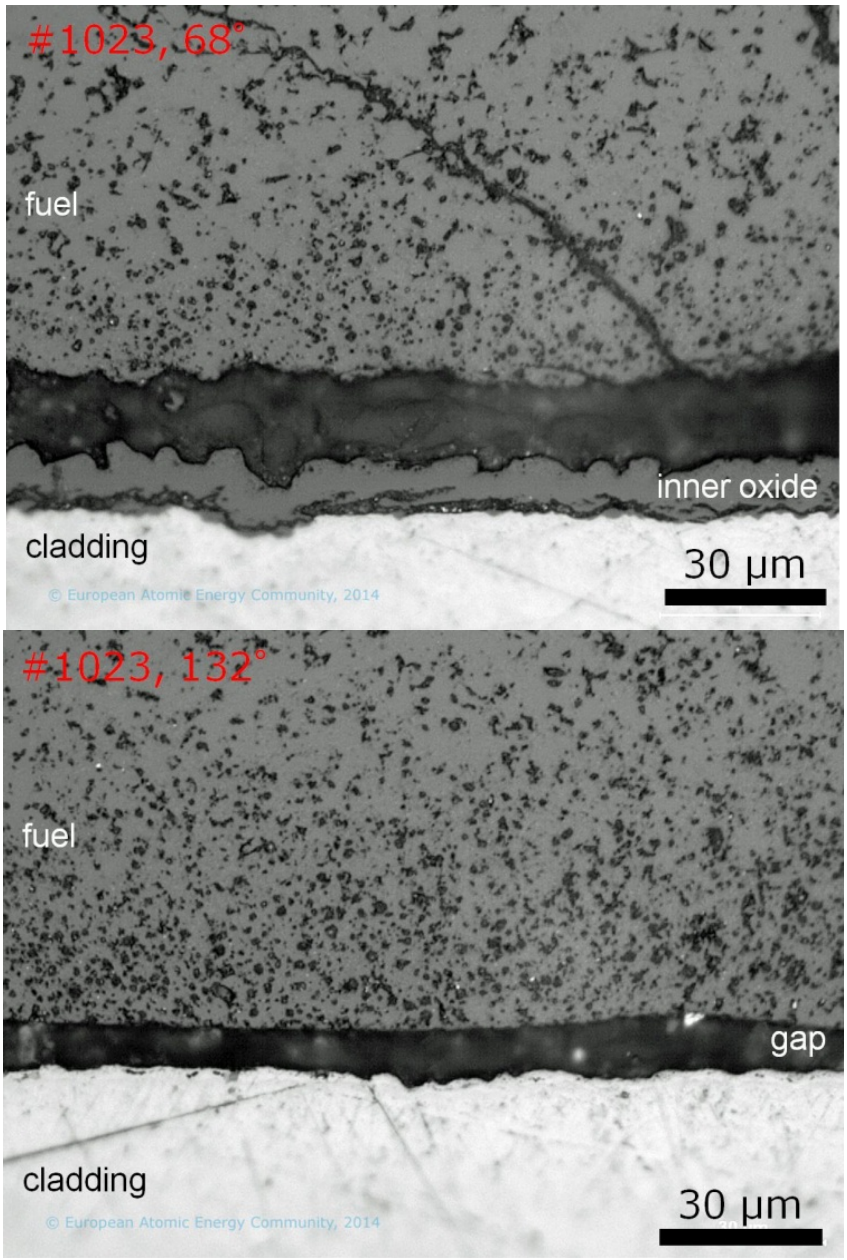

Figure 15: Micrographs of the PCI zones of the radial cut sample #1023 at 68°(upper image) and 132°(lower image).

6.4. Porosity

Porosity data were obtained by image analysis of 5 micrographs per radial profile and 2 profiles per sample. If possible the whole picture was used for analysis. Cracks, oxide layers and suspicious regions were excluded. At the pictures borders also partial pores were considered. The smallest area (approximately one pixel) taken into account is 0.02 μm^2.

Figure 16 shows a comparison of the radial pore number densities of all samples. The number of pores per area is constant from the centre to mid radius and increases then towards the periphery in case of the (#1021&#1022 average). The natural UO_2 (#1023 average) shows the same trend but is constant at the same level for ¾ of the radius before the pore number density

increases. At the periphery the absolute value is ~1.4 times lower than in case of the enriched UO_2 fuel.

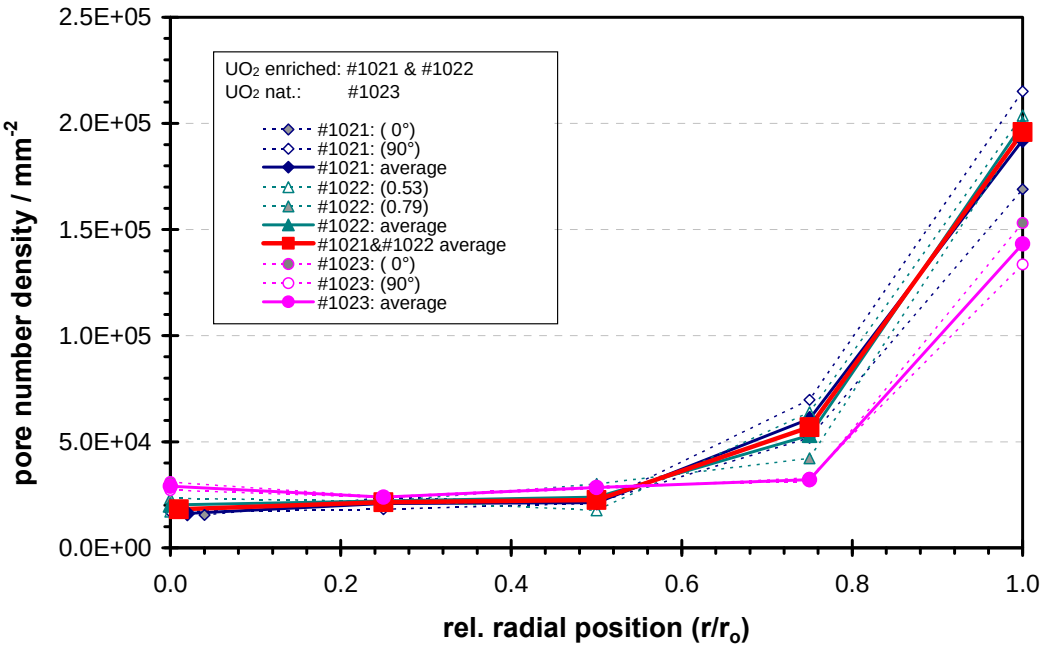

Figure 16: Comparison of radial pore number distributions of irradiated (3.8% ^{235}U) UO_2 fuel (#1021 and #1022) and irradiated natural (0.7% ^{235}U) UO_2 (#1023).

The porosity shows generally a similar behaviour. The porosity of fuels is near the centre around 5%. In case of the enriched fuel the porosity increases strongly from ¾ of the radius up to 20% at the periphery, while the porosity of natural fuel slowly increases from ¼ of the radius. In the rim zone at the periphery the porosity is high for both fuels. In case of the natural UO_2 the porosity is here 16% which is ~1.3 times lower than for the enriched fuel (20%). This behaviour reflects the differences in the burn-up of the samples.

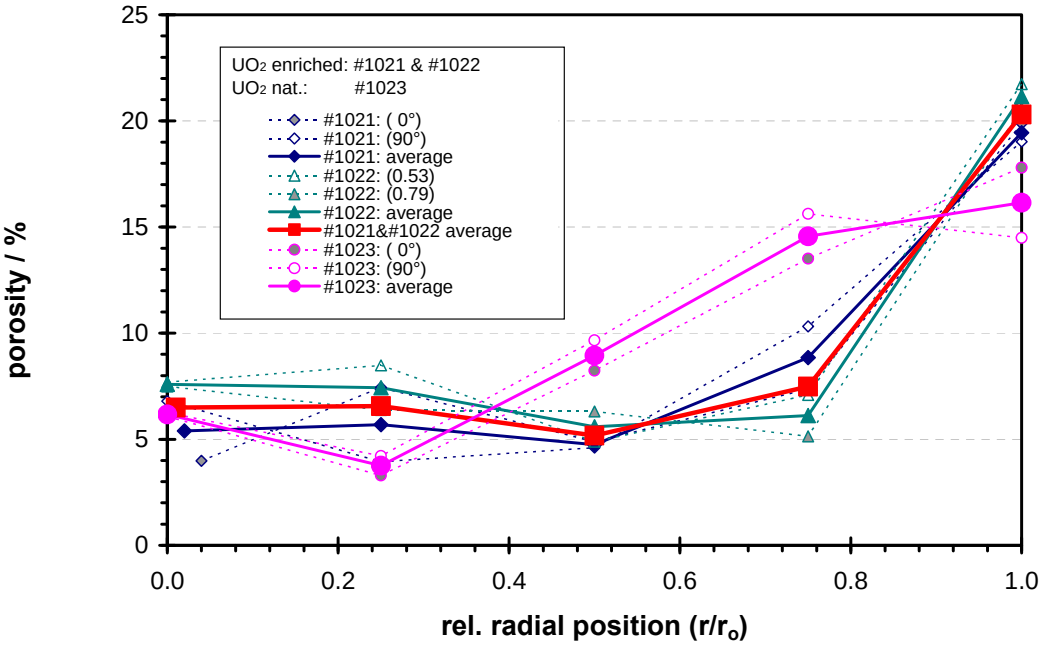

Figure 17: Comparison of radial porosity distributions of irradiated (3.8% ^{235}U) UO_2 fuel (#1021 and #1022) and irradiated natural (0.7% ^{235}U) UO_2 (#1023).

6.5. Metallic particles

Data on metallic inclusions in the fuel were obtained by the assumption that pure white spots seen in the micrographs are light reflections at metallic ε-particles. The data treatment was the same as in case of the porosity data. The smallest particle area (approximately one pixel) taken into account is 0.02 μm^2.

Both fuels show most of the metallic particles in the central part and very little in the intermediate part with a slight increase in the rim zone. In the irradiated natural UO_2 much less metallic particles are visible, as expected. In the centre is the particle number density the same for both fuels but the particles in the enriched fuel with higher local burn-up are 3 time larger in size. Towards the periphery the particle area decreases and stays constant from mid radius for natural UO_2 fuel (#1023 average) and from ¾ of the radius in case of the enriched UO_2 fuel (#1021 & #1022 average).

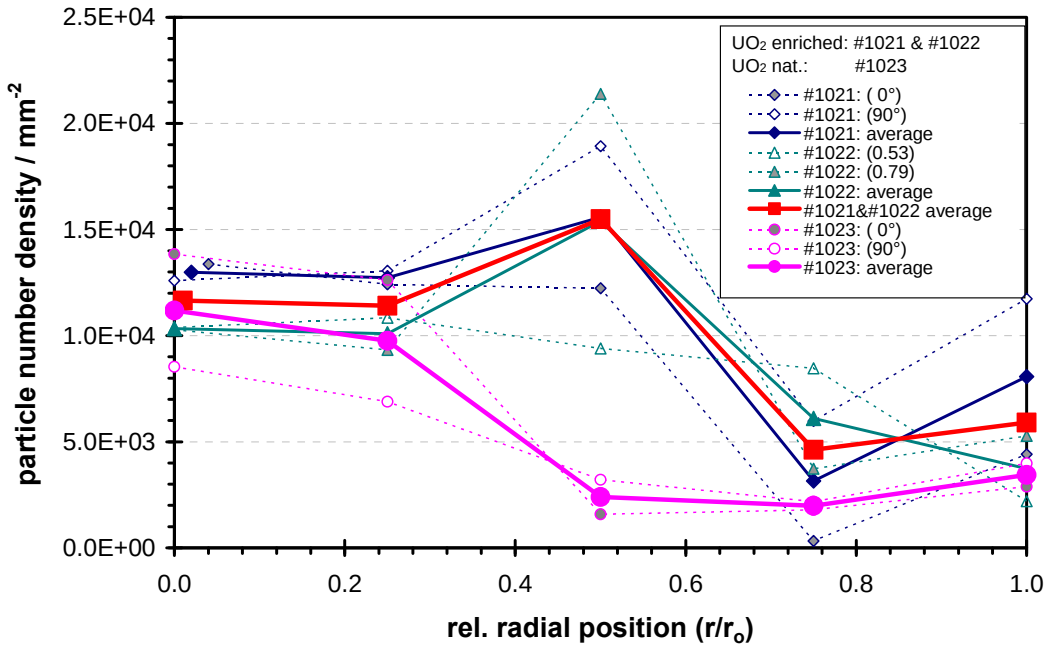

Figure 18: Comparison of radial distributions of particle number densities of irradiated (3.8% ^{235}U) UO_2 fuel (#1021 and #1022) and irradiated natural (0.7% ^{235}U) UO_2 (#1023).

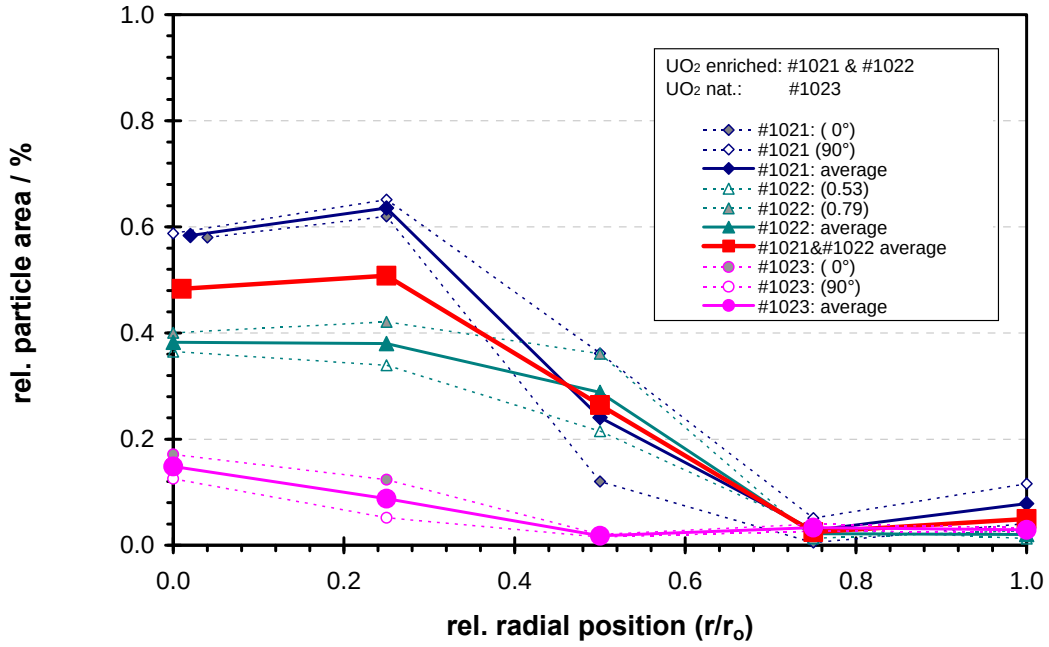

Figure 19: Comparison of radial distributions of relative particle areas of irradiated (3.8% ^{235}U) UO_2 fuel (#1021 and #1022) and irradiated natural (0.7% ^{235}U) UO_2 (#1023).

6.6. *Other findings*

Figure 20 show some unusual large dense zones which were detected mainly in the outer half of sample #1021.

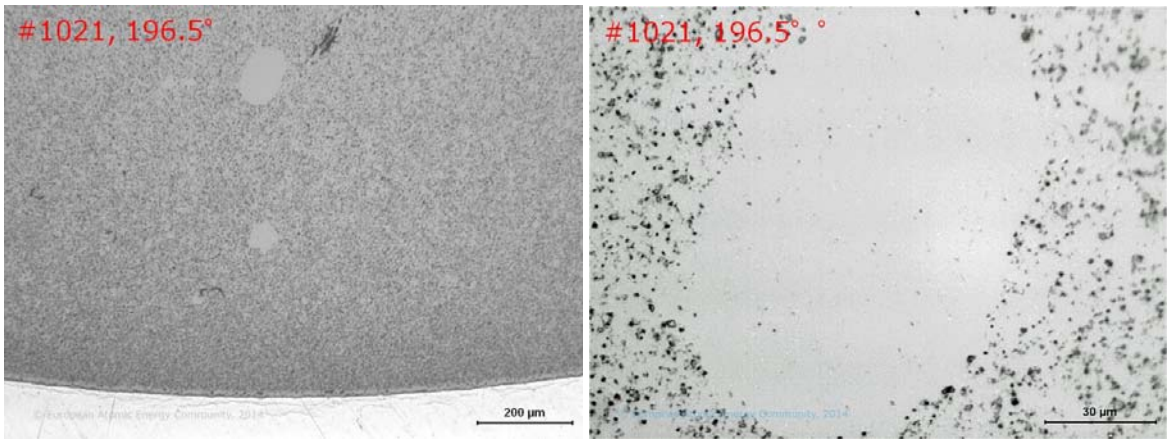

Figure 20: ***Sample #1021 shows some unusual large dense zones e.g. at 196.5° and r/r_o=0.89.***

Acknowledgement

The research leading to these results has received funding from the European Union's European Atomic Energy Community's (Euratom) Seventh Framework Programme FP7/2007-2011 under grant agreement n° 295722 (FIRST-Nuclides project).

7. References

[1] V. Metz, E. Bohnert, C. Bube, E. González-Robles, B. Kienzler, A. Loida, N. Müller, P. Carbol, J.-P. Glatz, R. Nasyrow, D. Papaioannou, V.V. Rondinella, D. Serrano Purroy, D. Wegen, H. Curtius, M. Klinkenberg, I. Günther-Leopold, C. Cachoir, K. Lemmens, T. Mennecart, J. Vandenborre, I. Casas, F. Clarens, J. de Pablo, R. Sureda Pastor, Z. Hózer, E. Slonszki, E. Ekeroth and O. Roth (2012). *Characterisation of spent nuclear fuel samples to be used in FIRST-Nuclides – relevance of samples for the Safety Case,* Deliverable No. 1.1 of the CP FIRST-Nuclides, Karlsruhe, Germany.

[2] V. Metz, E. González-Robles, N. Müller, E. Bohnert, M. Herm, M. Lagos, B. Kienzler, D. Serrano-Purroy, J.Y. Colle, O. Beneš, F. Naisse, T. Wiss, R.J.M. Konings, D.H. Wegen, D. Papaioannou, R. Gretter, R. Nasyrow, V.V. Rondinella, J.-P. Glatz, H. Curtius, H.W. Müskes, N. Like, D. Bosbach, I. Günther-Leopold, E. Curti, A. Froideval Zumbiehl, H.P. Linder, K. Govers, M. Verwerft, W. Van Renterghem, K. Lemmens, T. Mennecart, C. Cachoir, L. Adriaensen, A. Dobney, M. Gysemans, J. Vandenborre, A. Traboulsi, G. Blain, J. Barbet, M. Fattahi, R. Sureda Pastor, E. Slonszki, Z. Hózer and O. Roth (2013). *Characterisation of spent nuclear fuel samples and description of methodologies and tools to be applied in FIRST-Nuclides*, Deliverable No. 1.2 of the CP FIRST-Nuclides, Karlsruhe, Germany.

[3] Wegen, D. H., et al. (2014). *Characterisation of Commercial BWR Spent Fuel Samples for IRF Investigations and Oxygen Diffusion Experiments*. 2nd Annual Workshop Proceedings of the Collaborative Project "Fast/Instant Release of Safety Relevant Radionuclides from Spent Nuclear Fuel" (7th EC FP CP FIRST-Nuclides),Antwerp, Belgium, 05-07 November 2013. B. Kienzler, V. Metz, L. Duro and A. Valls. Karlsruhe, Germany, Karlsruhe Institute of Technology. KIT-SR 7676: 73-78.

[4] ASTM E321-96 (2012). *Standard Test Method for Atom Percent Fission in Uranium and Plutonium Fuel (Neodymium-148 Method)*, ASTM International, West Conshohocken, PA, 2012, www.astm.org

[5] P. De Regge and R. Boden (1977). *Determination of Neodymium Isotopes as Burn-up Indicator of Highly Irradiated (U,Pu)O_2 LMFBR Fuel*, *J. Radioanal. Chem.*, **35**, 173-184.

[6] Wegen, D. H., et al. (2012). *Non-destructive testing of segment N0204 of the spent fuel pin SBS1108*. JRC Scientific and Policy Report. Karlsruhe, Germany, European Commission, Joint Research Centre (JRC), Institute for Transuranium Elements (ITU). JRC 75272.

[7] Wegen, D. H., et al. (2013). *Preparation of Samples for IRF Investigations and Post Irradiation Examinations from 50.4 GWd/tHM PWR Fuel*. 1st Annual Workshop Proceedings of the Collaborative Project "Fast/Instant Release of Safety Relevant Radionuclides from Spent Nuclear Fuel" (7th EC FP CP FIRST-Nuclides), Budapest, Hungary, 09-11 October 2012. B. Kienzler, V. Metz, L. Duro and A. Valls. Karlsruhe, Germany, Karlsruhe Institute of Technology. KIT-SR 7639: 193-199.

[8] Wegen, D. H., et al. (2013). *Non-Destructive Analysis of a PWR Fuel Segment with a Burn-Up of 50.4 GWd/tHM – Part II: Defect Determination*. 1st Annual Workshop Proceedings of the Collaborative Project "Fast/Instant Release of Safety Relevant Radionuclides from Spent Nuclear Fuel" (7th EC FP CP FIRST-Nuclides),Budapest, Hungary, 09-11 October 2012. B. Kienzler, V. Metz, L. Duro and A. Valls. Karlsruhe, Germany, Karlsruhe Institute of Technology. KIT-SR 7639: 183-191.

[9] Wegen, D. H., et al. (2013). *Non-Destructive Analysis of a PWR Fuel Segment with a Burn-Up of 50.4 GWd/tHM – Part I: Visual Examination and Y-Scanning.* 1st Annual Workshop Proceedings of the Collaborative Project "Fast/Instant Release of Safety Relevant Radionuclides from Spent Nuclear Fuel" (7th EC FP CP FIRST-Nuclides),Budapest, Hungary, 09-11 October 2012. B. Kienzler, V. Metz, L. Duro and A. Valls. Karlsruhe, Germany, Karlsruhe Institute of Technology. KIT-SR 7639: 173-182.

[10] UTHSCSA ImageTool Version 3.0 (2002), developed at the University of Texas Health Science Center at San Antonio, Texas, http://compdent.uthscsa.edu/dig/itdesc.html